

Tuning correlation effects with electron-phonon interactions

J.P.Hague and N.d'Ambrumenil

Department of Physics, University of Warwick, CV4 7AL, U.K.

*We investigate the effect of tuning the phonon energy on the correlation effects in models of electron-phonon interactions using DMFT. In the regime where itinerant electrons, instantaneous electron-phonon driven correlations and static distortions compete on similar energy scales, we find several interesting results including (1) A crossover from band to Mott behavior in the spectral function, leading to hybrid band/Mott features in the spectral function for phonon frequencies slightly larger than the band width. (2) Since the optical conductivity depends sensitively on the form of the spectral function, we show that such a regime should be observable through the low frequency form of the optical conductivity. (3) The resistivity has a double kondo peak arrangement [Published as *J. Low. Temp. Phys.* **140** pp77-89 (2005)].*

PACS numbers: 71.10.Fd, 71.27.+a, 71.38.-k

1. Introduction

Mounting experimental evidence from high-T_c cuprates¹, nickelates², manganites^{3,4} and other interesting materials suggests that large electron-phonon interactions may play a more important role in the physics of strongly correlated electron systems than previously thought. Migdal-Eliashberg and BCS theories have proved extremely successful in describing the effects of phonons in many materials. However, if the coupling between electrons and the underlying lattice is large, and/or the phonons can not be treated within an adiabatic approximation, conventional approaches fail.

The Holstein model contains most of the fundamental physics of the electron-phonon problem⁵. Tight-binding electrons are coupled to the lattice through a local interaction with Einstein modes. For large phonon frequencies, electrons interact with a strongly correlated Hubbard-like attraction, while for small phonon frequencies the lattice gives rise to a static

potential which is essentially uncorrelated. Between these two extreme limits of correlated and uncorrelated behavior, levels of correlation are tuned by the size of the phonon frequency and novel physics is expected. In particular, it is normally the strength of interaction which is said to tune the correlation in e.g. the Hubbard model, whereas in the Holstein model, it can be seen that both interaction strength and phonon frequency may compete with each other to play this role.

The dynamical mean-field theory (DMFT) approach has proved successful in treating the Holstein and other models^{6,7,8}. DMFT treats the self-energy as a momentum-independent quantity and is accurate as long as the variation across the Brillouin zone is small. For many aspects of the electron-phonon problem in 3D, correlations are short ranged and DMFT can be successfully applied. The weak coupling phase diagram was studied by Ciuchi *et al.* where competing charge-order (CO) and superconducting states were found⁷. Freericks *et al.* developed a quantum Monte-Carlo (QMC) algorithm^{8,9} and examined the applicability of several perturbation theory based techniques to the electron-phonon problem^{10,11,12}. The prediction of measurable quantities away from certain well-defined limits is severely restricted owing to difficulties inherent in the analytic continuation. Dynamic properties such as spectral functions can be computed in the case of static phonons¹³, and close to the static limit¹⁴. Alternatively, the limit of high phonon frequency (attractive Hubbard model) has been studied with a QMC algorithm¹⁵.

In the current study we are concerned with the behavior of dynamical properties that could be measured directly with experiment. We use the iterated perturbation theory approximation, which has been demonstrated to be accurate for the Hubbard model, and use maximum entropy to analytically continue the results. We compare the resulting single-particle spectral functions over a wide range of electron-phonon coupling strengths and phonon frequencies. The results obtained using iterated perturbation theory (IPT) are promising and capture generic weak and strong coupling behavior for all phonon frequencies. At intermediate phonon frequencies, we find that electron-phonon interactions produce a spectral function which is simultaneously characteristic of both uncorrelated band (static) and strongly correlated Mott/Hubbard regimes. We also find that the competition between band-like and correlated states causes unusual structures in the optical conductivity and resistivity. Provided a material with high enough phonon frequency can be identified, it is possible that such a state could be observed experimentally.

This paper is organized as follows. First, we introduce the Holstein model, the dynamical mean-field theory and analytic continuation techniques

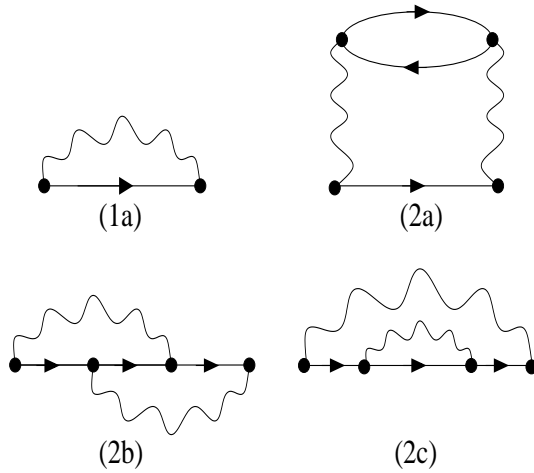


Fig. 1. Second order contributions to the self-energy. Straight lines represent electron Green's functions of the host and wavy lines phonon Green's functions.

(section 2.). In section 3., we use IPT to determine the spectral functions of the Holstein model. We compare IPT with exactly known results in the static limit. This, in conjunction with the conclusions of Ref. ¹¹ leads us to argue that IPT is a reasonable approximation for the calculation of dynamical properties in the intermediate phonon frequency regime. We compute the density of states, optical conductivity and resistivity, and give a heuristic explanation for their behavior.

2. Formalism

The Holstein Hamiltonian is written as,

$$H = -t \sum_{\langle ij \rangle \sigma} c_{i\sigma}^\dagger c_{j\sigma} + \sum_{i\sigma} (gx_i - \mu) n_{i\sigma} + \sum_i \left(\frac{M\omega_0^2 x_i^2}{2} + \frac{p_i^2}{2M} \right) \quad (1)$$

The first term in this Hamiltonian represents a tight binding model with hopping parameter t . The second term couples the local ion displacement, x_i to the local electron density. The final term can be identified as the non-interacting phonon Hamiltonian. c_i^\dagger (c_i) create (annihilate) electrons at site i , p_i is the ion momentum, M the ion mass, μ the chemical potential and g the electron-phonon coupling. The phonons are dispersionless with frequency ω_0 .

The perturbation theory of this model may be written down in terms

of electrons interacting via phonons with the effective interaction,

$$U(i\omega_s) = -\frac{g^2}{M(\omega_s^2 + \omega_0^2)} \quad (2)$$

Here, $\omega_s = 2\pi sT$ are the Matsubara frequencies for bosons and s is an integer. Taking the limit $\omega_0 \rightarrow \infty$, $g \rightarrow \infty$, while keeping the ratio g/ω_0 finite, leads to an attractive Hubbard model with a non-retarded on-site interaction $U = -g^2/M\omega_0^2$. Iterated-perturbation theory (IPT) is known to be a reasonable approximation to the half-filled Hubbard model^{16,17}. Taking the opposite limit ($\omega_0 \rightarrow 0$, $M \rightarrow \infty$, keeping $M\omega_0^2 \equiv \kappa$ finite) the phonon kinetic energy term vanishes, and the phonons depend on a static variable x_i . As such, the model may be considered as uncorrelated.

We solve the Holstein model using dynamical mean-field theory (DMFT). DMFT freezes spatial fluctuations, leading to a theory which is completely momentum independent, while fully including dynamical effects of excitations. In spite of this simplification, DMFT predicts non-trivial (correlated) physics and may be used as an approximation to 3D models¹⁸. As discussed in Ref. 6, DMFT involves the solution of a set of coupled equations which are solved self-consistently. The Green's function for the single site problem, $G(i\omega_n)$ can be written in terms of the self-energy $\Sigma(i\omega_n)$ as,

$$G^{-1}(i\omega_n) = \mathcal{G}_0^{-1}(i\omega_n) - \Sigma(i\omega_n), \quad (3)$$

where Σ is a functional of \mathcal{G}_0 , the Green's function for the host of a single impurity model. Here $\omega_n = 2\pi T(n + 1/2)$ are the usual Matsubara frequencies. The assumptions of DMFT are equivalent to taking the self-energy of the original lattice problem to be local, hence G is also given by,

$$G(i\omega_n) = \int \frac{d\epsilon \mathcal{D}(\epsilon_k)}{i\omega_n + \mu - \Sigma(i\omega_n) - \epsilon_k} \quad (4)$$

where $\mathcal{D}(\epsilon)$ the density of states (DOS) of the non-interacting problem (in our case $g = 0$). We work with a Gaussian DOS which corresponds to a hypercubic lattice¹⁸, $\mathcal{D}(\epsilon) = \exp(-\epsilon^2/2t^2)/t\sqrt{2\pi}$. Equations (3) and (4) are solved according to the following self-consistent procedure: Compute the Green's function from equation (4) and the host Green's function of the effective impurity problem, \mathcal{G}_0 , from equation (3); then calculate a new self-energy from the host or full Green's functions. In the following we will take the hopping parameter $t = 0.5$, which sets the energy scale.

Once the algorithm has converged, and after analytically continuing to the real axis, response functions can be computed. We use the MAXENT method for the determination of spectral functions from Matsubara axis

data. MAXENT treats the analytic continuation as an inverse problem ¹⁹. The Green's function, $G(z)$, is given by the integral transform,

$$G(z) = \int \frac{\rho(x)}{z-x} dx \quad (5)$$

where $\rho(x)$ is the spectral function ($\rho(\omega) = \text{Im}[G(\omega + i\eta)]/\pi$). The problem of finding ρ is therefore one of inverting the integral transform. Since the data for G_n are incomplete and noisy for any finite set of Matsubara frequencies, the inversion of the kernel of the discretised problem is ill-defined. The MAXENT method selects the distribution $\rho(x)$ which assumes the least structure consistent with the calculated or measured data. These methods have been extensively reviewed in the context of the inversion of the kernel in Refs. 19,20. The applicability to the current problem has been thoroughly tested, and is found to be accurate.

Within the DMFT formalism, many response functions follow directly from the one-electron spectral function and the electron self-energy (essentially because of the neglect of all connected higher point functions apart from \mathcal{G}_0). Here we will be interested in the conductivity ⁶:

$$\text{Re}[\sigma(\omega)] = \frac{\pi^2}{\omega} \int_{-\infty}^{\infty} d\epsilon \mathcal{D}(\epsilon) \int_{-\infty}^{\infty} d\nu \rho(\epsilon, \nu) \rho(\epsilon, \nu + \omega) [f(\nu) - f(\nu + \omega)] \quad (6)$$

where $f(x)$ is the Fermi-Dirac distribution. Taking the limit, $\omega \rightarrow 0$, leads to the DC conductivity. (The conductivity is in units of $e^2 V / \hbar a^2$, where a is the lattice spacing, V the volume of the unit cell and e and \hbar are the electron charge and Planck's constant respectively.)

3. Results

In this section, we examine the validity of an approximation to the self-energy constructed from only first and second order terms with respect to the spectral functions calculated at very high and very low phonon frequencies. Finally, we calculate the optical conductivity and resistivity.

Spectral functions are shown in figures 2 and 3. The perturbation theory is carried out in the host Green's function (i.e. both electrons and phonons are bare). All diagrams in fig. 1 are considered,

$$\Sigma_{1a}(i\omega_n) = -UT \sum_s \mathcal{G}_0(i\omega_n - i\omega_s) D_0(i\omega_s) \quad (7)$$

$$\Sigma_{2a}(i\omega_n) = -2U^2 T^2 \sum_{s,m} D_0^2(i\omega_{n-m}) \mathcal{G}_0(i\omega_m) \mathcal{G}_0(i\omega_s) \mathcal{G}_0(i\omega_{n-m+s}) \quad (8)$$

$$\Sigma_{2b}(i\omega_n) = U^2 T^2 \sum_{s,m} D_0(i\omega_{m-s}) D_0(i\omega_{n-m}) \mathcal{G}_0(i\omega_m) \mathcal{G}_0(i\omega_s) \mathcal{G}_0(i\omega_{n-m+s}) \quad (9)$$

$$\Sigma_{2c}(i\omega_n) = U^2 T^2 \sum_{s,m} D_0(i\omega_{n-m}) D_0(i\omega_{m-s}) \mathcal{G}_0^2(i\omega_m) \mathcal{G}_0(i\omega_s) \quad (10)$$

This also gives the correct weak coupling limit for the electronic Green's function.

We consider first the calculation of spectral functions close to the static and Hubbard limits. In the instantaneous limit the perturbation theories for the Holstein and Hubbard models are equivalent. It is well known that second order perturbation theory in the host Green's function provides a good approximation to the Hubbard model²¹. In the static limit, the exact solution can easily be calculated¹³. Figure 2 shows spectral functions from the exact solution, computed for a hypercubic lattice and spectral functions, computed using 2nd order perturbation theory at a temperature of $T = 0.08$. The phonon frequency $\omega_0 = T/20$ was chosen so that the effects of the phonon kinetic energy are negligible compared to thermal fluctuations. This allows a direct comparison to be made between the exact and approximate results. The comparison shows that the widths and positions of the major features are closely related.

The results in Figure 2 for the static limit ($\omega_0 \rightarrow 0$), together with the fact that second order IPT is known to give reasonable results in the instantaneous limit ($\omega_0 \rightarrow \infty$), suggest that the calculation of spectral functions should also be reliable at intermediate frequencies. We note that Freericks *et al.* also find a reasonable agreement between the IPT and QMC self-energies at half-filling, and that this should lead to a good agreement in the Matsubara axis Green's function. We have therefore solved the IPT equations for the spectral functions at intermediate frequencies. We show the results in Fig 3.

The results of the IPT calculations in the regime of intermediate coupling (Fig 3) are consistent with known results for the limiting cases. For frequencies $\omega \gg \omega_0$, the system has the qualitative behavior of the static limit: The original unperturbed density of states splits into two sub-bands centered around $\pm U/2$. For small frequencies ($\omega \ll U, \omega_0$) and interaction strength, U , less than some critical value, the system behaves as an interacting electron (Hubbard) model, since the retarded interaction between particles $U(i\omega_s)$ (see equation 2) is effectively constant for $\omega_s \ll \omega_0$. There is then a narrow quasiparticle band at the Fermi energy with density of states at the Fermi energy pinned at its non-interacting value⁶. We also note that the results for small coupling and small frequencies are in good agreement with those calculated using ME theory in the metallic phase²².

The recent renormalization group (NRG) calculations of Meyer *et al.*

^{23,24} also report the spectral function in the intermediate regime. The NRG is in principle an exact method for solving the impurity problem onto which the DMFT equations map. Our results are largely consistent with theirs adding further support to the use of IPT in the intermediate regime. When comparing with the results of Meyer *et al* ²³, one should note that the Hamiltonian (1) is exactly the one considered in Ref. 23 but with the quantity $g/\sqrt{2M\omega_0} = \sqrt{U\omega_0}/2$ denoted by g in Ref. 23 and with energies measured in terms of the full bandwidth (instead of the half-bandwidth used here). In this paper, we work with the Gaussian density of states for the non-interacting electron DOS, whereas reference 23 uses the semi-elliptic DOS. In general, we would expect the critical values for the opening of a gap to be larger for the Gaussian case than for the semi-elliptic case. The critical coupling for the parameters in Figure 3(c) lies just above $U = 2.0$, corresponding in the units used in Ref. 23 to $g = 1$, compared with the critical value found for the semi-elliptic DOS of $g = 0.69$ (note that because of the different energy scales $\omega_0 = 2$ in our results corresponds to $\omega_0 = 1$ in the units of 23). However, the shapes of the spectral functions are similar in both cases, with a five-peaked structure below and four peaked structure above the transition. The peaks are narrower in the IPT results than in the NRG results and there is less weight in the high energy peaks. This may reflect the different DOS, or inaccuracies in the NRG method at frequencies far from the Fermi energy resulting from the logarithmic discretisation, but more likely the limitations of the IPT method.

Using the method outlined in section 2. it is possible to calculate the real-axis self-energy. The temperature evolution of the imaginary part of the self-energy may be seen in figure 4 for $U = 2$ and $\omega_0 = 2$. The self-energy at low temperatures and small frequencies shows a quadratic (Fermi-liquid like) behavior consistent with the narrow quasiparticle peak seen in the spectral function (Fig 3) and develops to a broad central peak at higher temperatures. There are also peaks corresponding to the Hubbard sub-bands. With increasing temperature these phonon-induced peaks move together and merge into the single central maximum associated with incoherent on-site scattering. This peak is naturally characterized within the framework of the self-consistent impurity model formulation of the DMFT equations ⁶ in terms of a Kondo resonance. In this formulation, the dynamical mean field $\mathcal{G}_0(\omega)$ is written in terms of a hybridization $\Delta(\omega)$ between the site orbital and a bath of conduction electrons and is therefore equivalent to an Anderson impurity model with the added complication that Δ is frequency-dependent and needs to be computed self-consistently. However, many of the properties in the metallic state are similar to those of the Anderson impurity model. In particular the central peak in the spectral function can be viewed as the

Kondo resonance of the impurity model.

As all connected point-functions with order higher than \mathcal{G}_0 are neglected within DMFT, the computation of $q = 0$ response functions is straightforward. As an example we show in fig 5 the (real part of the) optical conductivity for various temperatures with $U = 2$ and $\omega_0 = 2$. The structure seen in the curves reflects the structure of the density of states. There is a strong response at low frequencies as particle-hole pairs are excited within the ‘Kondo-like’ quasiparticle resonance at the Fermi energy. The second peak at frequencies $\omega \sim 1$ arises from excitations between the quasiparticle resonance and the large satellite (Hubbard band), while the third peak around $\omega \sim 5.0$ involves excitations between the satellites. The first dip at $\omega = 0.5$ is the signature of the small Mott bands close to the Kondo resonance and is the feature most likely to be observable experimentally.

Also calculated is the resistivity as a function of temperature (figure 6). The curves reflect the structure of the self-energy shown in Figure 4: At low temperatures the resistivity rises quadratically as expected for interacting electrons. The temperature scale is given by the quasiparticle bandwidth (‘Kondo temperature’). Above this temperature the resistivity drops as the on-site (Kondo) scattering amplitude for electrons reduces. There is a slight second peak at higher temperatures. The structures in ρ can be traced back to the behavior seen in the self-energy. This second peak is the result of an increase in scattering off the phonons: these soften slowly with increasing temperature and, around the second peak in the resistivity curve, outweigh the reduction in Kondo-like scattering as the temperature increases. This effect clearly involves a partial cancellation between two effects and hence may be sensitive to the accuracy of the analytic continuation, which at higher temperatures starts from reduced information (since the majority of Matsubara points simply show asymptotic behaviour).

4. Summary

We have discussed the result of changing the ratio of electron and phonon energies as a method for tuning the amount of correlation in a model of electron-phonon interactions. We use approximate schemes to solve for the spectral functions of the Holstein model. On the basis that second-order iterated perturbation theory predicts the correct qualitative behavior at a range of couplings in the static limit as well as describing correctly the limit of infinite phonon frequency, we have computed the spectral function at intermediate frequencies and couplings. We have used an adaptation of the standard maximum entropy scheme to obtain the spectral function, the self-

energy and the conductivity of the model by analytic continuation. These quantities had not previously been studied.

The results for the intermediate frequency regime are consistent with what might be expected on the basis of the limiting cases (high and low frequencies). At energy scales smaller than ω_0 , the system shows behavior similar to that of the Hubbard model found in the instantaneous limit $\omega_0 \rightarrow \infty$: there is a narrow central ‘Kondo-resonance’ or quasiparticle band. At large energies the model behaves as it does in the static regime with a well-defined band splitting. At intermediate frequencies the picture is complicated by the interplay of the loss of coherence in the quasiparticle band and the effective renormalization of the phonon frequency as a function of coupling and temperature. We suggest that if systems with anomalously large phonon frequencies and couplings exist, then the optical conductivity should bear the hallmark of the correlation tuned regime.

5. Acknowledgements

The authors would like to thank F.Essler and F.Gebhard for useful discussions.

REFERENCES

1. A.Lanzara, P.V.Bogdanov, X.J.Zhou, S.A.Kellar, D.L.Feng, E.D.Lu, T.Yoshida, H.Eisaki, A.Fujimori, K.Kishio, J.-I.Shimoyama, T.Noda, S.Uchida, Z.Hussa, and Z.-X.Shen. *Nature*, 412:6846, 2001.
2. J.M.Tranquada, K.Nakajima, M.Braden, L.Pintschovius, and R.J.McQueeney. Bond-stretching-phonon anomalies in stripe-ordered $\text{La}_{1.69}\text{Sr}_{0.31}\text{NiO}_4$. *Phys. Rev. Lett.*, 88:075505, 2002.
3. G.M.Zhao, K.Conder, H.Keller, and K.A.Müller. *Nature*, 381:676, 1996.
4. A.J.Millis, R.Mueller, and B.I.Shraiman. *Phys. Rev. B*, 54:5405–5417, 1996.
5. T.Holstein. *Ann. Phys.*, 8:325–342, 1959.
6. A.Georges, G.Kotliar, W.Krauth, and M.Rozenburg. *Rev. Mod. Phys.*, 68:13, 1996.
7. S. Ciuchi, F.de Pasquale, C.Masciovecchio, and D.Feinberg. *Europhys. Lett.*, 24:575–580, 1993.
8. J.K.Freericks, M.Jarrell, and D.J.Scalapino. *Phys. Rev. B*, 48:6302–6314, 1993.
9. J.K.Freericks, M.Jarrell, and D.J.Scalapino. *Europhys. Lett.*, 25:37–42, 1994.
10. J.K.Freericks. *Phys. Rev. B*, 50:403–417, 1994.
11. J.K.Freericks and M.Jarrell. *Phys. Rev. B*, 50:6939–6952, 1994.
12. J.K.Freericks, V.Zlatic, W.Chung, and M.Jarrell. *Phys. Rev. B*, 58:11613–11623, 1998.

13. A.J.Millis, R.Mueller, and B.I.Shraiman. *Phys. Rev. B*, 54:5389–5404, 1996.
14. P.Benedetti and R.Zeyher. *Phys. Rev. B*, 58:14320–14334, 1998.
15. M.Keller, W.Metzner, and U.Schollwock. Dynamical mean-field theory for the normal phase of the attractive hubbard model. *J. Low. Temp. Phys*, 126:961, 2002.
16. A.Georges and G.Kotliar. *Phys. Rev. B*, 45:6479, 1992.
17. M.J.Rozenberg, X.Y.Zhang, and G.Kotliar. *Phys. Rev. Lett.*, 69:1236, 1992.
18. W.Metzner and D.Vollhardt. *Phys. Rev. Lett.*, 62:324, 1989.
19. J.E.Gubernatis, M.Jarrell, R.N.Silver, and D.S.Sivia. *Phys. Rev. B*, 44:6011, 1991.
20. H.Touchette and D.Poulin. Aspects numériques des simulations du modèle de hubbard – monte carlo quantique et méthode d’entropie maximum. Technical report, Université de Sherbrooke, 2000.
21. X.Y.Zhang, M.J.Rozenberg, and G.Kotliar. *Phys. Rev. Lett.*, 70:1666, 1993.
22. J.P.Hague and N.d’Ambrumenil. *cond-mat/0106355*, 2001.
23. D.Meyer, A.C.Hewson, and R.Bulla. Gap formation and soft phonon mode in the holstein model. *Phys. Rev. Lett.*, 89:196401, 2002.
24. A.C.Hewson and D.Meyer. Numerical renormalization group study of the anderson-holstein impurity model. *J. Phys. Condens. Matt*, 14(3):427, 2002.

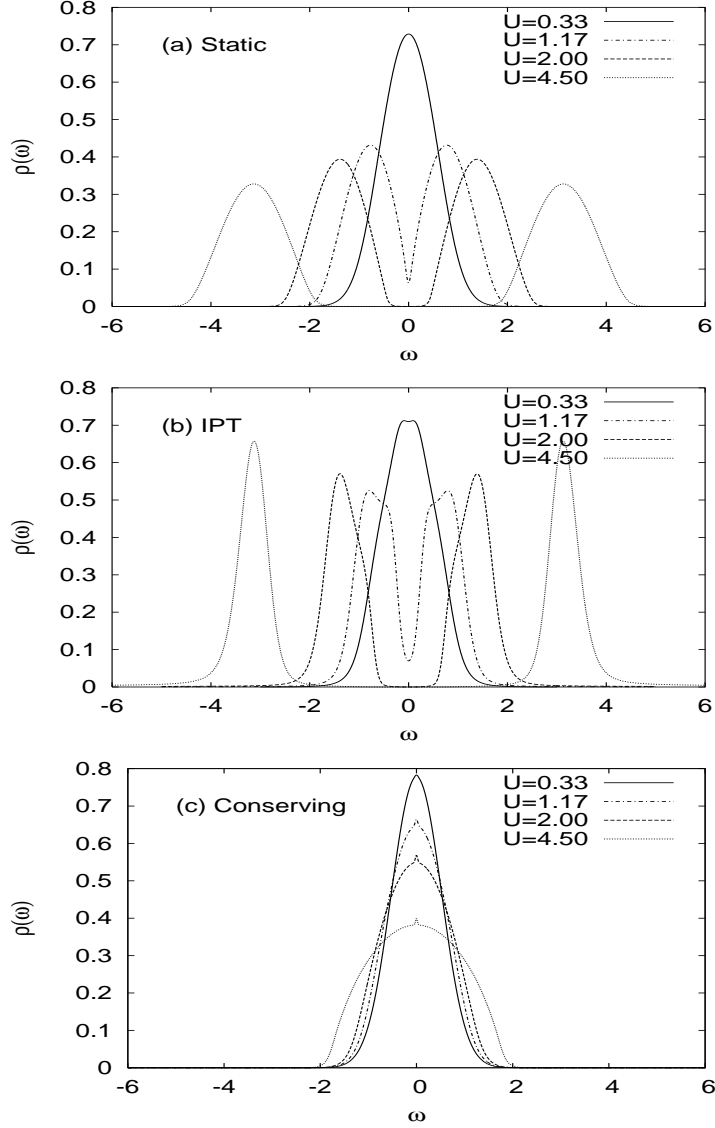


Fig. 2. The spectral function in the static limit of the half-filled Holstein model computed at temperature $T = 0.08$ (a) using the exact solution and (b) using 2nd order IPT at a low frequency, $\omega_0 = 0.004$. The IPT solution at this small non-zero frequency is quite close to the exact solution in the static limit. In particular, the band splitting and the positions of the maxima agree. To contrast, panel (c) shows the results of the approximation using the full Green's function (Diagram 2c from figure 1 is not included to avoid overcounting)

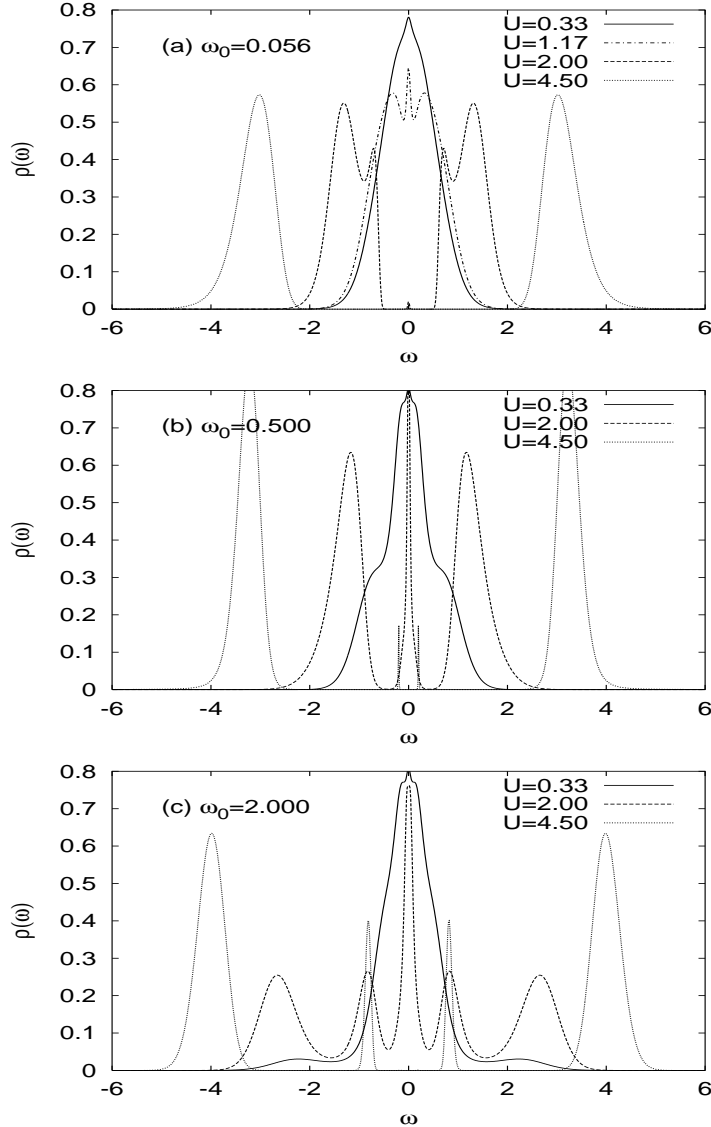


Fig. 3. Spectral functions of the half-filled Holstein model for various electron-phonon couplings U , approximated using 2nd order perturbation theory at $T = 0.02$ and $\omega_0 = 0.056$ (top), $\omega_0 = 0.5$ (center) and $\omega_0 = 2$ (bottom). In the low frequency limit ($\omega_0 = 0.125$), the spectral functions are similar to those in the static limit shown in Fig. 2, with only a small effect from the non-zero phonon frequency. As the temperature is lower than the phonon frequency, the central quasiparticle peak is clearly resolved for $U \leq 2$. For the intermediate frequencies (central panel) the peak around $\omega = 0$ is again clear and has a width $\sim \omega_0$ at low coupling. In the gapped phase at large couplings two band-splittings are visible. For $\omega \gg \omega_0$ the band splits just as in the static limit, while for $\omega \ll U$ there is a peak at a renormalized phonon frequency (which is less than the bare phonon frequency). In the ungapped phases for $\omega_0 = 0.5$ and 2 , the low energy behavior is similar to that found in the Hubbard model with a narrow quasiparticle band forming near the Fermi energy with the value at the Fermi energy pinned to its value in the non-interacting case.

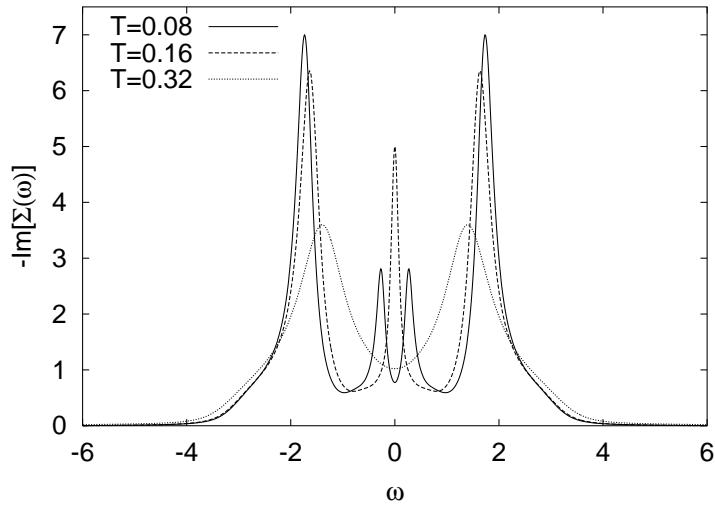


Fig. 4. Imaginary part of the self-energy of the half-filled Holstein model when $U = 2$ and $\omega_0 = 2$ computed using IPT and analytically continued using MAXENT. At low temperatures the low frequency behavior is Fermi-liquid like (quadratic dependence on ω) down to quite low frequencies (at very low frequencies and low temperatures there are some inaccuracies associated with the truncation in Matsubara frequencies). There are peaks at the frequencies associated with the phonon energy and with U . As the temperature increases the minimum at the Fermi energy ($\omega = 0$) increases as incoherent on-site scattering in the corresponding local impurity increases (see text). At temperatures above the characteristic (Kondo-like) energy scale the central peak subsides and disappears.

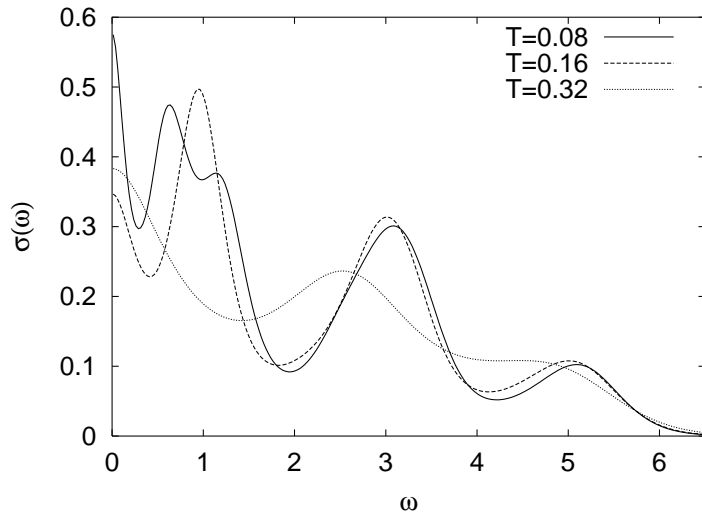


Fig. 5. The real part of the optical conductivity for a system with $U = 2.0$ and $\omega_0 = 2.0$ for a range of temperatures. The structure of the spectrum reflects that in the density of states (see fig 3). At low frequencies, electrons may be excited within the quasiparticle resonance. The second peak at $\omega \sim 2.0$ represents excitations from the Kondo resonance to the large satellite (Hubbard band), and the peak at $\omega \sim 5.0$ represents excitations between the satellites.

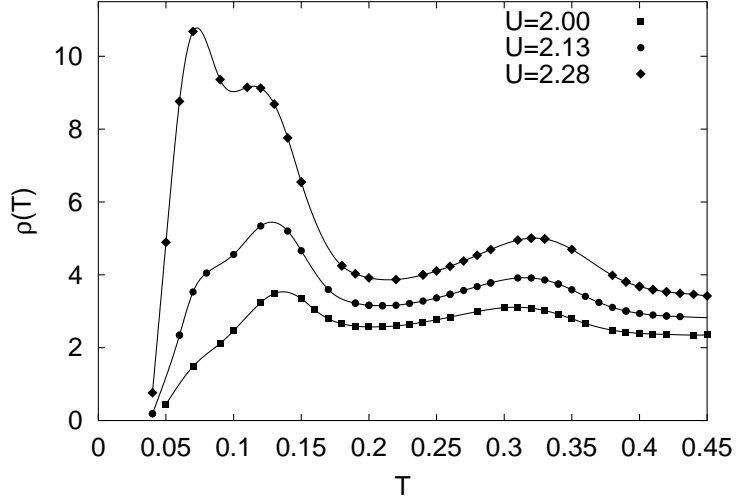


Fig. 6. The resistivity as a function of temperature for the Holstein model for $\omega_0 = 2$ for varying electron-phonon coupling strengths. The resistivity is in units of e^2V/ha^2 with V the unit cell volume and a the lattice cell spacing. The behavior reflects what is seen in the self-energy. At low temperatures the behavior is similar to that in a Kondo lattice. The resistivity rises sharply with temperature for temperatures smaller than the quasiparticle bandwidth. The resistivity then drops for temperatures larger than this lattice coherence temperature. A simple logarithmic decay with temperature is not visible because, in addition to the Kondo-like scattering processes, the electrons are scattered from thermally excited phonons whose spectral weight broadens and shifts towards lower frequencies as the temperature rises. This leads to a second peak. In contrast, the second peak is not visible for the Hubbard model, and indicates the presence of two energy scales in the Holstein model.